

# Workload Behavior Driven Memory Subsystem Design for Hyperscale

Suyash Mahar\*, Hao Wang<sup>†</sup>, Wei Shu<sup>§</sup>, Abhishek Dhanotia<sup>‡</sup>

\*UC San Diego <sup>†</sup>NVIDIA <sup>§</sup>Tenstorrent <sup>‡</sup>Meta Inc.

## Abstract

Hyperscalars run services across a large fleet of servers, serving billions of users worldwide. These services, however, behave differently than commonly available benchmark suites, resulting in server architectures that are not optimized for cloud workloads. With datacenters becoming a primary server processor market, optimizing server processors for cloud workloads by better understanding their behavior has become crucial. To address this, in this paper, we present MemProf, a memory profiler that profiles the three major reasons for stalls in cloud workloads: code-fetch, memory bandwidth, and memory latency. We use MemProf to understand the behavior of cloud workloads at Meta and propose and evaluate micro-architectural and memory system design improvements that help cloud workloads' performance.

MemProf's code analysis shows that cloud workloads at Meta execute the same code across CPU cores. Using this, we propose shared micro-architectural structures—a shared L2 I-TLB and a shared L2 cache. Next, to help with memory bandwidth stalls, using workloads' memory bandwidth distribution, we find that only a few pages contribute to most of the system bandwidth. We use this finding to evaluate a new high-bandwidth, small-capacity memory tier and show that it performs  $1.46\times$  better than the current baseline configuration. Finally, we look into ways to improve memory latency for cloud workloads. Profiling using MemProf reveals that L2 hardware prefetchers, a common solution to reduce memory latency, have very low coverage and consume a significant amount of memory bandwidth. To help improve future hardware prefetcher performance, we built a memory tracing tool to collect and validate production memory access traces.

## 1. Introduction

Over the last few years, the market share of the cloud as a portion of the total server market has constantly been increasing. Cloud deployments now account for  $>50\%$  of the total server processor market and are expected to grow even further [29, 22]. However, CPU benchmarks available today do not accurately represent cloud workloads' microarchitectural and memory system behavior, leaving the processors largely unoptimized for their unique characteristics.

Cloud workloads show different behavior than the CPU benchmarks available today across several metrics. For one, the fleet-wide IPC for major hyperscalars is significantly lower than the benchmark suites [27, 15]. With millions of servers running these workloads, even small improvements in IPC from understanding the behavior of these workloads can result

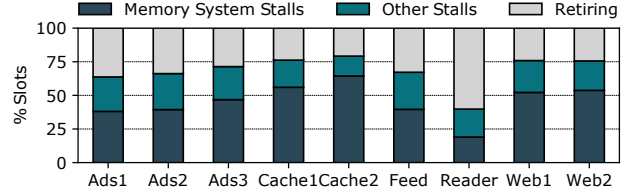


**Figure 1: Breakdown of where the CPU pipeline slots spend their time across nine production workloads using top-down analysis [31].**

in significant cost savings and efficiency improvements across the fleet.

To improve the performance of cloud workloads, in this paper, we study and characterize nine microservices serving live production traffic. These microservices represent a diverse range of workloads at a hyperscaler's datacenters and run on a large portion of the fleet.

Figure 1 presents the top-down analysis [31] of the nine workloads at Meta to show that the memory system is the primary reason for CPU pipeline stalls that leads to low instructions per cycle (IPC) of cloud workloads. Memory system-related stalls can have three sources, (1) stall on an instruction fetch (*code-fetch bound*), (2) stall on the memory system with a high request pending queue occupancy (*memory bandwidth bound*), or (3) stall on the memory system with a low request pending queue occupancy (*memory latency bound*).

To dive further into these three sources of stalls in cloud workloads, we created a new tool, MemProf, that enables detailed profiling of workloads' micro-architectural and memory system behavior. We use observations from MemProf to propose and evaluate new micro-architectural changes and system architecture for cloud server processors.

Code fetch-related stalls are a significant problem in cloud workloads [2, 27]. Using MemProf, we observe workloads at Meta run similar code and share page table mappings across cores. Building on this observation, we propose sharing the L2 Cache and L2 I-TLB among a small cluster of CPU cores (e.g., four) that are physically close. Shared micro-architectural structures for instructions help reduce code-fetch stalls by enabling the cores running similar code to pool their caches for a larger apparent cache size even though they have the same per-core cache size.

Memory bandwidth is another significant contributor to memory system stalls. Over the years, the DDR memory capacity and bandwidth have been scaling at very different rates [20]. Increasing memory bandwidth and capacity disparity, along with growing core counts in modern server processors has resulted in limited per-core memory bandwidth,

requiring processors to populate more memory channels, thus resulting in higher server TCO. We use MemProf to study the memory bandwidth distributions of production workloads and find that only a small percentage of pages contribute to most of the memory bandwidth utilization across the workloads. We use this observation to propose and evaluate new tiered memory systems where a small, high-bandwidth memory tier serves the bandwidth needs of the workload. In contrast, a low-bandwidth, large-capacity tier provides additional memory capacity, lowering the total cost of ownership (TCO) of the servers. We find that by splitting the memory capacity in 30:70% between the high-BW and low-BW tiers, we can achieve  $1.46\times$  better throughput and 13% better throughput/cost than the baseline DDR-only configuration.

Finally, we look into ways to improve memory latency for cloud workloads. Using MemProf, we observe that although L2 hardware prefetchers improve memory latency by prefetching cachelines, they often have very low coverage in real-world cloud workloads, resulting in minor IPC improvements. Further, we observe that L2 hardware prefetcher’s inefficiencies result in high memory bandwidth consumption, exacerbating the memory bandwidth problem. A major hurdle in optimizing these hardware prefetchers is access to the cloud workloads to study their memory behavior. To enable broader access to cloud workloads’ behavior, we collect memory access traces from production workloads to help future hardware prefetcher research.

This paper is the first to study how cloud workloads interact with the memory system and to use these observations to propose shared  $\mu$ -arch structures and memory bandwidth tiering. While previous works from Google [2, 15] and Meta [27, 26] have looked into the  $\mu$ -arch behavior of the hyperscale workloads, they have not performed detailed studies of the code behavior, memory bandwidth distribution, or hardware prefetcher efficiency. In summary, in this paper, we make the following contributions:

- **Detailed study and characterization of cloud workloads.** We perform a detailed study of the code, memory bandwidth, and memory latency trends at Meta.
- **New profiling methodology and tool.** We present MemProf, a profiling tool for cloud workloads, to understand their interaction with the memory system.
- **Code sharing across cores.** We show that CPU cores run very similar code across all the workloads, enabling performance improvements from shared  $\mu$ -arch resources.
- **Memory bandwidth distribution.** We study the memory bandwidth distribution, find that very few pages contribute to a large amount of bandwidth and propose new tiered memory solutions for cloud workloads.
- **Hardware prefetcher efficiency.** We observe that L2 hardware prefetchers have significant memory bandwidth overhead and small performance improvements. To mitigate this, we collect memory traces from production workloads to help future hardware prefetcher research.

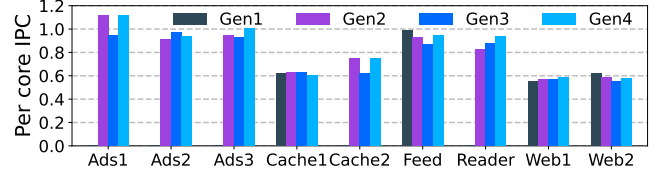


**Figure 2: Generation over generation IPC change for the nine workloads. Some services do not run on the Gen1 servers and thus miss their IPC data.**

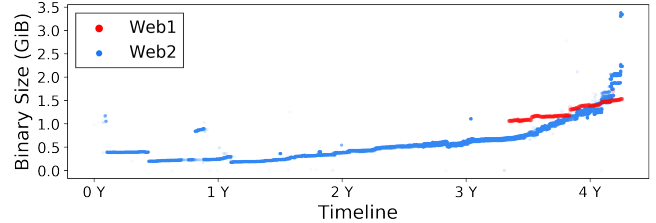


**Figure 3: Binary Size trend for Web1 and Web2. Web2 binary size increased by  $5.6\times$  over the last four years.**

In the next section, we look into the three reasons for memory system stalls: code fetch, memory bandwidth, and memory latency. We follow with description of MemProf and use it to make observations and proposals in each area.

## 2. Code, Memory BW, and Latency Challenges in Cloud Datacenters

Existing benchmarks that are generally used to design processors do not accurately represent the workloads at hyperscalars. As highlighted by several previous works [2, 4, 15, 27, 26], because of the fundamentally different behavior of cloud workloads, they show significantly different IPC, cache miss rate, and other metrics than standard benchmarks. These factors make the SPEC and other commercially available benchmarks a bad proxy for studying the performance of server processors in a datacenter.

To understand how the IPC has changed over the years at Meta, we chart nine representative cloud workloads’ IPC over four server generations. Figure 2 shows that cloud workloads have very small or even negative IPC improvement between server generations, motivating the need to understand cloud workloads better to optimize server processors for hyperscalars.

To understand the reasons for this inhibited performance growth of server processors running cloud workloads, we will look into each of the three primary reasons for memory system stalls and understand how they affect cloud workloads’ performance.

### 2.1. Increasing Code Footprint of Datacenter Applications

Cloud workloads are often frontend bound due to their large code footprint, resulting in high instruction cache miss rates [2]. The code footprint can be several 100s of MiBs and has been increasing over the years. Figure 3 shows the increase

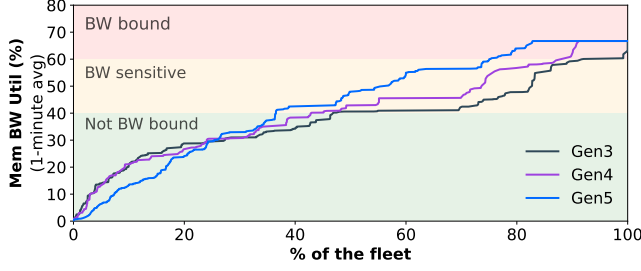


**Figure 4: Fleet memory bandwidth utilization (%) across three generations (1-minute average) as a CDF. BW bound and BW sensitive regions are based on the memory bandwidth vs latency characteristics of DDR memories.**

in the binary size for Web1 and Web2, the two major web services at Meta over the years. Web2 shows an exponential increase in binary size, a  $5.6\times$  increase over four years.

In contrast, the I-cache sizes have stayed relatively constant (32KB I\$ per core) across several server generations and have only recently started increasing on some server architectures. Likewise, instruction TLB lookups are optimized for the latency-sensitive instruction fetch pipeline, which makes it harder for them to scale with the rapidly growing code footprints of cloud workloads. Previous work on cloud workload has observed a similar code-footprint trend. Kanev et al. [15] show that the code footprint at Google is growing at a rate of 27% per year. This imbalance between the processor’s micro-architectural resources and the growing code footprint have resulted in frontend to be the leading source of bottleneck for many workloads across several server generations and resulted in stagnant IPC over time. These trends necessitate new processor micro-architecture optimization.

## 2.2. Memory Bandwidth Scaling Challenge

Memory bandwidth is another major concern for cloud workloads, resulting from poor DRAM bandwidth scaling and increasing CPU core count. To understand cloud workloads’ memory bandwidth utilization trend, we show the fleet-wide memory bandwidth consumption increase over the three generations of servers in Figure 4. With the most recent generation (Gen 5), the 1-minute average memory bandwidth utilization shows that majority of the fleet is either bandwidth sensitive or bandwidth bound. While micro-benchmarks can generally push memory bandwidth utilization to  $>80\%$ , we observe that production workloads are rarely able to push memory bandwidth utilization beyond 60% utilization as any further increase results in exponential increase in memory latency [24]. Thus, we classify workloads with higher than 60% bandwidth utilization as memory bandwidth bound (shaded red in Figure 4). Likewise, workloads with average memory bandwidth utilization between 40%-60% can have high transient memory bandwidth utilization and are thus classified as memory BW sensitive. While the fleet-wide data is 1-minute average, transient peaks can make these workloads significantly bandwidth bound during shorter time intervals causing tail latency spikes

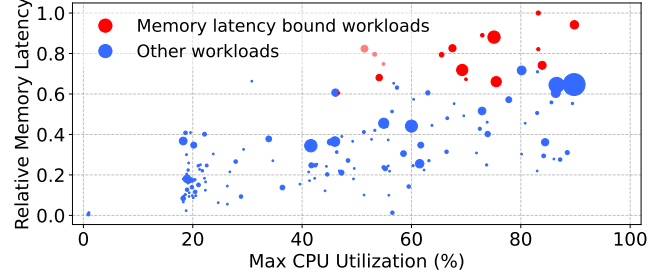


**Figure 5: Relative memory latency vs. max CPU utilization for microservices across the fleet. Services, where latency SLO constraints bind CPU utilization are shown in red. Marker size is scaled by service’s relative size.**

and limiting overall system CPU utilization.

Besides growing memory bandwidth utilization across the fleet, increasing disparity between DIMM’s bandwidth and capacity [20] makes alleviating memory bandwidth problems of cloud workloads harder as hyperscalars need to provision a large number of memory channels and DIMMs per server for sufficient memory bandwidth.

This trend towards growing memory bandwidth utilization and poor bandwidth scaling of DDR-based memories necessitates a better way to provision memory in cloud datacenters and curb the cost and power consumption of the servers [10].

## 2.3. High Memory Latency Leading to CPU Underutilization

Finally, many cloud workloads are memory latency sensitive as they must meet requests’ latency service level objectives (SLOs) [11]. These workloads run at the maximum CPU utilization possible without violating SLO guarantees, often wasting CPU resources. Memory latency limits CPU utilization as increase in memory latency lowers system’s IPC. Lower IPC for workloads results in cloud workloads spending more cycles doing “on-cpu” work, and thus results in longer query response times.

To study this trend across the fleet, Figure 5 shows the max CPU utilization vs. relative memory latency of workloads using a scatter plot. We make three important observations from the fleet-wide data: (a) Memory latency increases significantly with increasing CPU utilization. That is, a large portion of the fleet is operating at a relatively high memory latency ( $>0.5$ ). (b) Workloads marked in red have 20-50% stranded CPU cores because of the latency SLO constraints. These workloads need to leave CPU cores idle to avoid violating SLO guarantees, resulting in wasted resources and inefficiency at datacenter scale. (c) And, differences in memory access patterns (e.g., bursty memory load) results in workload to have different memory latency at similar CPU utilizations.

Hardware prefetching is one of the key techniques used in modern server processors to hide memory latency. L2 hardware prefetchers, however, have a significant memory bandwidth overhead. From our analysis in Section 6, we find that

workloads show a substantial increase in total memory bandwidth consumption with L2 prefetchers enabled while providing limited performance gains, signaling that the prefetchers have low efficiency.

Next, we will present our profiling tool, MemProf, to characterize cloud workloads and use it to explore opportunities for performance improvements in cloud server processors.

### 3. MemProf

So far, we have looked at the sources and implications of memory system stalls. To understand how to mitigate these overheads, we will present MemProf, a code and memory profiler, to profile and understand the memory subsystem behavior of cloud workloads. MemProf is an automated tool that measures several hardware counters, samples events using Intel PEBS [7], and generates reports regarding code sharing, memory bandwidth distribution, and memory latency behavior.

#### 3.1. Design

Figure 6 shows the overview of MemProf. MemProf has three components that measure the three aspects of memory system-related stalls. (1) *MemProf.Code* measures the code behavior of a workload to understand code sharing across cores and code bandwidth distribution. (2) *MemProf.MemBW* generates the memory bandwidth distribution to help understand how hot memory pages in a system are. And, (3) *MemProf.MemLat* generates data to understand the effectiveness of common techniques in reducing memory latency.

#### 3.2. Methodology

Next, we will look at the methodology used by MemProf and understand its working.

**MemProf.Code** For profiling the code behavior of workloads, MemProf samples per-core L1 I-TLB miss events (`FRONTEND_RETIRED.L1I_MISS`) using Intel precise event-based sampling (PEBS). Larger granularity sampling using I-TLB miss events enables MemProf to cover wider address space regions. Further, I-TLB-based miss sampling and dense binary layout of hot code using link-time optimization [23] enable low frequency, low-overhead code footprint estimation.

With the I-TLB miss event samples, MemProf computes the hit distribution across the address space of the workload and uses it to generate the code heatmap, code bandwidth distribution, and compute the correlation between the miss events of two cores (Figure 6a). For all these calculations, MemProf uses the virtual address of the samples.

MemProf.Code’s results help understand the code footprint and code sharing across cores in cloud workloads.

**MemProf.MemBW** To understand the memory bandwidth requirements of a workload, MemProf samples the precise LLC demand load miss event (`MEM_LOAD_RETIRED.L3_MISS`) and generates the memory

Table 1: Gen 4 system configuration.

Parameter	Value
Cores/Threads	26/52
L1 I-/D-Cache	32 KiB/core each, private
L2 Cache	1 MiB/core, unified, private
I-L1 TLB	2 MiB/4 MiB pages fully assoc., 8 entries/thread; 4 KiB pages 8-way, 128 entries/core
LLC	1.375 MiB/core

bandwidth distribution profile for a workload (Figure 6b). Since Intel processors report virtual addresses for miss samples, MemProf translates the virtual address (VA) to physical address (PA) using the workload’s page table and uses the resulting physical address for computing the memory bandwidth distribution. MemProf supports sampling over a configurable interval to study memory bandwidth trends over time and translates the samples’ address at the end of the sampling interval. In cases where the page table entries for an address range might not exist at the end of a measurement interval, MemProf keeps around the last copy of the page table and uses it to translate any addresses missing in the current copy.

**MemProf.MemLat** To measure how effective hardware prefetchers are in reducing memory latency, MemProf performs two sets of measurements. To compute their accuracy and coverage, MemProf measures the cache and prefetcher-related hardware counters and uses the following expressions. (CL = cachelines, pref. = prefetched)

$$Accuracy = 1 - \frac{(Unused\ pref.\ CLs\ evicted)}{(Total\ pref.\ CLs)}$$

$$Coverage =$$

$$\frac{(Total\ pref.\ CLs) - (Unused\ pref.\ CLs\ evicted)}{(Total\ CLs\ brought\ in) - (Unused\ pref.\ CLs\ evicted)}$$

To measure the memory bandwidth overhead of enabling L2 hardware prefetchers, MemProf measures the total system bandwidth consumption and IPC with L2 prefetchers enabled and disabled across all cores. Since these counters are only available for L2 caches, MemProf only generates accuracy and coverage data for L2 prefetchers.

Collecting accuracy, coverage, and memory bandwidth overhead of L2 hardware prefetchers gives us insights into the behavior of the prefetchers with different workloads.

#### 3.3. Production Servers and Workloads

We run containerized production workloads on bare metal machines (that is, no hypervisor or virtual machines) to characterize microservices in Section 3, and for studies in Section 4 and 5. These workloads represents a large part of the datacenter fleet and exhibit a wide range of  $\mu$ -architectural behaviors. We run each of these workloads near peak load operating point. Peak load is determined as the max throughput the workload can sustain without violating any SLOs.



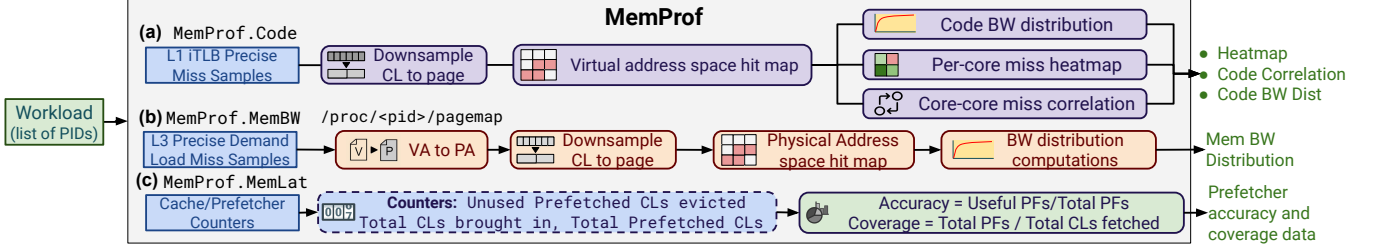


**Figure 6: MemProf overview. (a) MemProf.Code, (b) MemProf.MemBW, (c) MemProf.MemLat profile the code, memory BW, and memory latency behavior, respectively.**

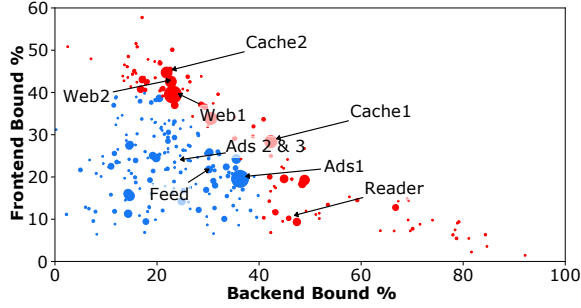


**Figure 7: Distribution of workloads across the fleet based on % frontend and backend stalls. Marker size is scaled by the workload's server count.**

Further, all experiments were run on the fourth generation of servers, with the hardware configuration listed in Table 1.

We use nine representative workloads running live production traffic to study the frontend and backend behavior of the fleet. Figure 7 shows the percentage of CPU pipeline slots across the microservices that are frontend and backend bound. Across the fleet, we see that workloads show extremely diverse  $\mu$ -arch behavior, ranging from highly frontend bound to highly backend bound.

The nine labeled microservices in the scatter plot account for a significant portion of the fleet and exhibit diverse  $\mu$ -arch behavior. We study these nine workloads in our work to perform a representative characterization of cloud workloads at Meta.

These microservices are Web1, Web2, Ads1, Ads2, Ads3, Cache1, Cache2, Feed, and Reader. To achieve the maximum query rate for Cache1, hosts use 2/3 of the cores for running the workload. The rest of the 1/3 cores are used for network processing and handling NIC IRQs. Most microservices spawn multiple threads, where only one thread is assigned to a logical core. In contrast, Web2 spawns multiple processes and assigns up to one process per logical core.

## 4. Code Behavior of Cloud Workloads

As we showed in Section 2, stalls in the CPU frontend pipeline due to instruction cache and TLB misses are a significant fraction of the memory system stalls across the nine workloads. To mitigate the code-fetch overhead, in this section, we look at the code access behavior of cloud workloads at the full system level and propose  $\mu$ -arch optimizations.

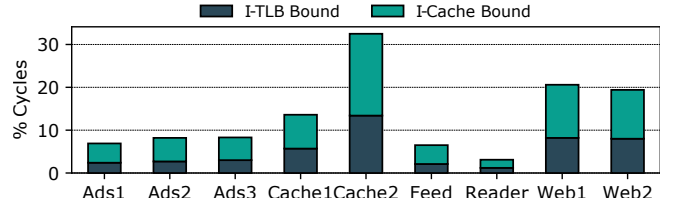


**Figure 8: % of cycles bound by code fetch (I-cache and I-TLB).**

To understand the impact of a large code footprint, Figure 8 shows the percentage of all CPU cycles where the CPU core was stalled waiting for an I-TLB miss or an I-cache miss. Web1, Web2, and Cache2 spend over 20% of their cycles stalling on instruction fetch. This code fetch overhead is a direct result of the rapid footprint growth of cloud workload binaries due to their high development velocities, as shown in Figure 3 for Web1 and Web2 workloads. Although, we use huge pages and code layout optimization techniques [6, 23] to reduce I-TLB and I-cache misses, we still see fairly high frontend stalls. This is partly because application developers do not control huge page usage and code layout for many dynamically linked libraries; and because the code footprint is too large and still growing.

To help mitigate the code-fetch overhead, using MemProf, we make the key observation that cloud applications run very similar code on different CPU cores, in terms of both the virtual and physical address spaces, and for both multi-threaded and multi-process applications.

### 4.1. Working Set Size for Code

Next, we will look at the code bandwidth and footprint of the nine workloads to understand why they are significantly code-fetch bound.

Using MemProf.Code's L1 I-TLB miss event measurements; we generate the code bandwidth of the workloads, as shown in Figure 9. We find that all workloads have very large code footprints, with one notable example being the Web1 workload, which has a code footprint of 125 MiB.

We further investigate the effects of the large code footprint by measuring the L1-L3 cache code miss rate. Figure 10 shows the code MPKI for the three levels of caches. For the nine workloads, we see that the large footprint of cloud workloads results in a high code miss rate across all three levels, with Web1 and Web2 even fetching a significant amount of code lines from memory.

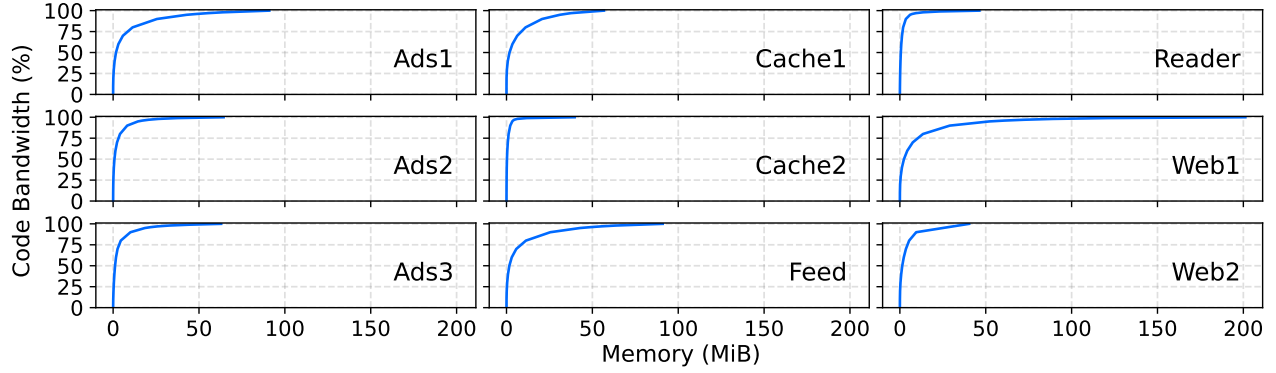


**Figure 9: Code bandwidth distribution for the nine production workloads using precise L1 I-TLB miss events. X-axis represents code pages sorted by their hotness and the Y-axis shows the relative memory bandwidth contribution of the ‘X’ MiB of hottest pages.**

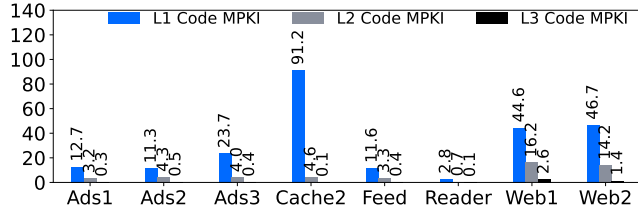


**Figure 10: L1, L2, and L3 cache code misses per kilo-instruction.**

Using Figure 9 and Figure 10, we make three important observations: (a) despite the recent server processors trends resulting in larger last-level cache (LLC), large (albeit infrequently accessed) code footprint of some workloads (Figure 9) results in diminishing returns in LLC code MPKI improvements. (b) Second, extremely large L1 code MPKI values suggest that active code footprint greatly exceeds the L1 code sizes. (c) Finally, workloads like Cache2 can show abnormally high L1 cache MPKI and code-fetch bound cycles despite a relatively smaller code footprint. Investigating further, we found that Cache2 suffers from a high branch misprediction rate resulting in it being significantly more code-fetch bound.

It is interesting to note that, workloads show a  $\sim 10\times$  reduction in code MPKI from L2 to L3, which is much higher than the L1-to-L2 reduction. While considering the capacity, L2 is often  $32\times$  of L1 while per-core L3 is only about  $1.35\times$  of L2. This suggests that code benefit from shared L3 and effectively uses much more capacity than its per-core quota would suggest.

#### 4.2. Code-Sharing Behavior for Cloud Workloads

So far, we have looked into the code-fetch overhead of cloud workloads and the resulting performance loss; next, we will present our observation that cloud workloads running across cores share code cachelines, allowing shared cache structures to improve the workload’s performance.

To understand if the cores are accessing identical address locations, using MemProf, we sampled the L1 I-TLB miss events for different cores running the same workload. Figure 11a shows the I-TLB miss heatmap for two cores running

**Table 2: Pearson correlation between Core0 and Core1 for L1 I-TLB miss events.**

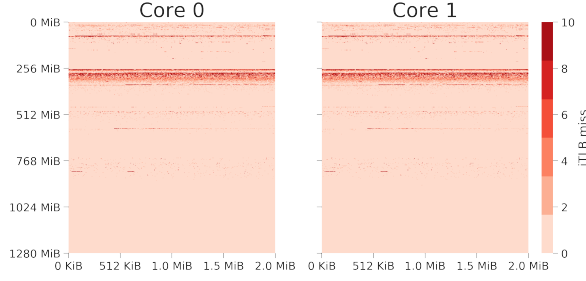
Workload	Corr. value	Workload	Corr. value
Web1	0.9997	Web2	0.9881
Ads1	0.9977	Ads2	0.9921
Ads3	0.9833	Feed	0.9977
Cache1 b/w workload cores	0.9947	Cache1 b/w NIC cores	0.9168
Cache1 b/w workload & NIC	0.0010	Cache2	0.9978
Reader	0.9887		

the Web1 workload for the first 1.28 GiB of the address space. Across the address space, both cores show very similar code access patterns, suggesting that the cores are accessing common code pages. We test our hypothesis by computing the Pearson correlation coefficient for the two cores; the Web1 workload shows a correlation value of 0.9997. A Pearson correlation value close to 1 suggests that the L1 I-TLB miss events for both cores are highly correlated, and thus, the cores have very similar code access patterns.

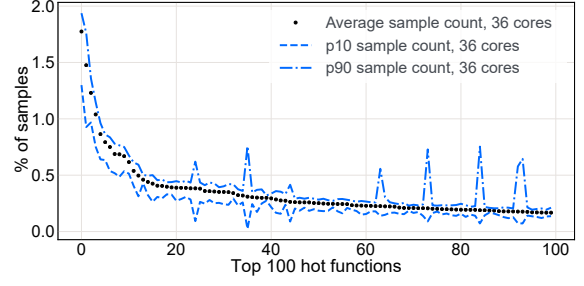
Table 2 shows a similar trend for the other workloads. All nine workloads show a high correlation between cores for L1 I-TLB miss events.

For multithreaded workloads, accessing the same pages implies that the CPU cores access common mappings across threads. For the Web2 microservice that spawns multiple processes, we use the page table to verify that code page mappings have the same translation across processes. For Web2, we observe common code mappings across processes as all child processes spawn from the same parent.

To confirm that cores are executing the same code, we collect stack samples across all cores and check if they execute the same functions. Figure 11b shows the average, p90, and p10 weight of the top 100 functions across all the cores for the Web1 workload. The L1 I-TLB miss correlation and cores executing identical functions across them confirm that the CPU cores execute identical code, leading to our first key observation.



(a) L1 I-TLB miss event distribution for the address space of Web1. Each row represents a 2 MiB slice of the address space. Contiguous rows represents a contiguous part of the address space.



(b) Hot functions across cores for Web1 stack sampling.

Figure 11: Code sharing across cores using MemProf.

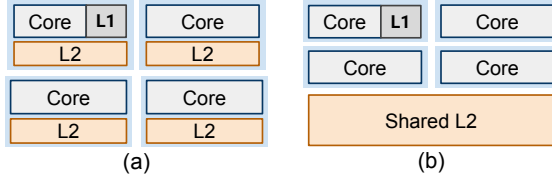


Figure 12: Shared cache design with unified L2 cache shared among four cores. (a) Private 1 MiB/core L2. (b) Shared, 1 MiB/core shared L2 (total 4 MiB) cache.

**Key observation 1:** Cores run similar code across them.

Using this observation about cloud workloads, we will propose two new  $\mu$ -arch improvements and evaluate their effectiveness using the Web1 workload. We chose the Web1 workload as it is significantly frontend bound (Figure 7) and runs across a large portion of the fleet.

#### 4.3. Reducing I-Cache Misses Using a Shared L2 I-Cache

Since the CPU cores share code; with a shared L2 cache, the cores will see an increased apparent cache size for shared cachelines. To take advantage of this, we propose using a shared L2 architecture (Figure 12) where a cluster of four cores shares a unified L2 cache. To keep the hardware cost similar, we propose the per-core L2 cache size stay similar. Thus, for a processor resembling the Gen4 platform (Table 1) should share 4 MiB of L2 cache among four cores (1 MiB/core).

**4.3.1. Evaluation Methodology** To evaluate the performance improvements from a shared L2 cache, we use Intel’s L2 CAT [9] and CDP [8] to measure and project how Web1’s performance changes with increasing code cache size.

While using simulations can allow us to closely model the shared cache design, simulations suffer from several limitations. For example, full-system or system-call emulations have significant performance overhead which changes application’s runtime behavior. While trace-based simulations can have lower overhead, they cannot accurately capture the timing characteristics, inter-thread dependencies, or RPCs, making them impractical for cloud workloads.

Table 3: Evaluated system configuration for cache scaling.

Parameter	Value
I-L1 Cache	32 KiB/core, private
L2 Cache	2 MiB/core, unified, private
LLC	1.875 MiB/core

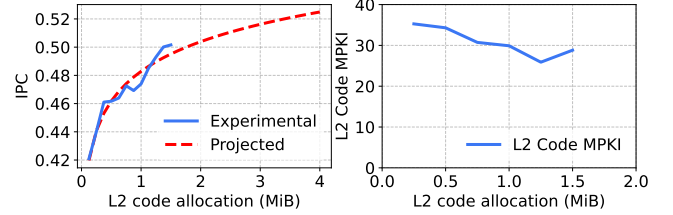


Figure 13: IPC scaling and projection along with L2 code MPKI change for Web1 with increasing L2 code cache allocation.

**4.3.2. Results** Figure 13 shows the measured and projected IPC along with the L2 code MPKI for the Web1 workload serving live traffic. We use a machine with the cache configuration listed in Table 3 and scale the L2 code partition from 128 KiB to 1.5 MiB while keeping the L2 data partition constant at 0.5 MiB (50% of Gen4 L2\$, based on our study of code-data split in L2 cache). To project performance beyond 1.5 MiB code partition, we extrapolate the experimental data using linear projection in logspace. We chose this projection to model the cache behavior where the performance improves linearly with an exponential increase in cache size [1].

The Web1 workload shows a 9.1% performance improvement when the cache size increases from 0.5 MiB (50% of private 1 MiB L2 cache) to 2 MiB (50% of shared 4 MiB L2 cache), that is,  $4\times$  increase in apparent code cache size.

Thus, based on code sharing across cores and the performance increase from a larger code cache for Web1, one of the most frontend bound workloads, we observe that cloud workloads benefit from a larger shared L2 cache.

#### 4.4. Reducing I-TLB Misses with a Shared L2 I-TLB

Similar to a shared L2 cache, we propose a shared L2 I-TLB to exploit common page mappings for code across cores for cloud workloads. Figure 14 shows a shared L2 I-TLB archi-

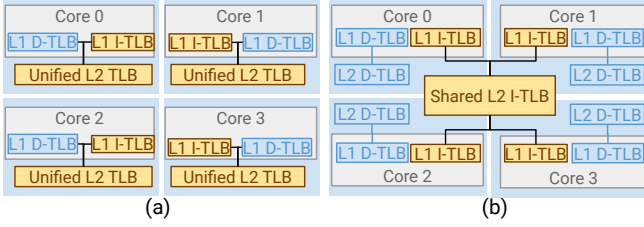


**Figure 14: Shared L2 I-TLB design with unified L2 cache shared among 4 cores. (a) Private 1 MiB/core unified L2. (b) Shared, 1 MiB/core Unified L2 (total 4 MiB) cache.**

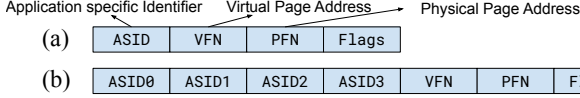


**Figure 15: TLB entry design for (a) private TLB (b) shared TLB.**

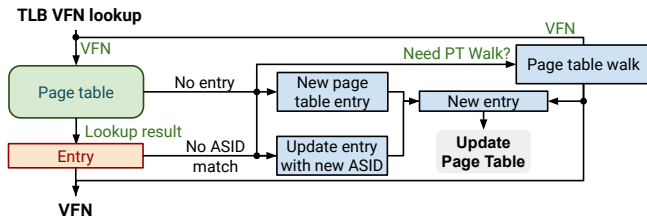
ture where a cluster of four cores shares the L2 I-TLB, but each core still has a private L2 D-TLB. A shared L2 I-TLB allows the cores running identical code to share the TLB entries, making a larger number of TLB entries available to the workload.

Supporting shared I-TLB for multithreaded programs requires no additional changes to the TLB entries. Each TLB entry includes an ASID (Figure 15a) to track which process the entry belongs to. Since each CPU core is part of the same address space in multithreaded programs, the shared unmodified TLB entries can support multiple cores.

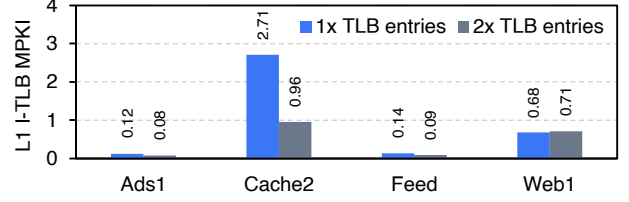
For multiple processes across cores, we propose the shared I-TLB entries to include multiple ASIDs (Figure 15b). For our design, we propose 4 processes to share a single L2 I-TLB; thus, each TLB entry only needs 4 ASIDs, one for each core.

Figure 16 shows the mechanism for a TLB lookup and to install a new entry if it does not already exist. When a translation request comes into the TLB, if the virtual address (VFN) and the entry’s application-specific ID (ASID) match, the corresponding physical address (PFN) is returned. If the entry for the VFN does not exist, or the entry’s ASIDs do not match the request, the TLB performs a page table walk and adds a new entry or updates the existing page table entry.

**4.4.1. Evaluation Methodology** Next, we will validate whether cloud workloads benefit from larger I-TLB sizes by changing the L1 I-TLB entry count to  $2\times$ . We are unable to do the similar scaling study as Section 4.3, because the cache partitioning feature is not available for TLBs. Further, as previously stated,  $\mu$ -arch simulators cannot capture the behavior of production environment making detailed architecture



**Figure 16: Page table lookup and update for a shared L2 I-TLB.**



**Figure 17: I-TLB MPKI with  $1\times$  and  $2\times$  L1 I-TLB entries for four cloud workloads.** simulation impractical.

**4.4.2. Results** Figure 17 shows the change in L1 I-TLB MPKI when the number of entries is doubled, showing that workloads benefit from an increased I-TLB size. To increase the count of I-TLB entries, we measure per-thread L1 I-TLB MPKI with simultaneous multithreading (SMT) on ( $1\times$  entries) and off ( $2\times$  entries).

Thus, shared code mappings and an increase in performance with more L1 I-TLB entries show that cloud workloads benefit from a larger, shared L2 I-TLB. While a larger I-TLB results in a lower MPKI, shared TLB can still suffer from trashing over smaller time intervals if the threads sharing the TLB are in different application phases.

## 5. Understanding and Improving Memory Bandwidth

The challenges of memory bandwidth scaling and limited per-DIMM bandwidth have resulted in cloud workloads being more memory bandwidth-bound (Section 2.2). Current server processors only support a single memory tier; thus, hyperscalars need to populate more DRAM channels to meet the memory bandwidth needs. This results in higher power consumption and wasted memory capacity at the datacenter scale.

Recent memory industry trends have resulted in new memory technologies like HBM and HB-DIMMs that can be directly connected to the CPUs to deliver high bandwidth. These technologies present a potential to explore memory bandwidth tiering as a solution to the bandwidth and capacity scaling challenges.

In this section, we will study the memory bandwidth characteristics of cloud workloads and look at the potential of high bandwidth memory technologies in improving cloud workloads’ performance and server TCO at Meta.

### 5.1. Memory Bandwidth Distribution

Using MemProf, we measured the memory bandwidth distribution over 30, 60, and 120 seconds. Figure 18 shows the amount of memory contributing to different bandwidth percentiles. Across the nine workloads, we observe that over 30 seconds, the active memory footprint is less than 25% of the total memory capacity, while the 90%-tile bandwidth is contributed by less than 10% of the memory capacity. Moreover, a similar memory bandwidth profile for different measurement intervals suggests that the memory bandwidth distribution re-



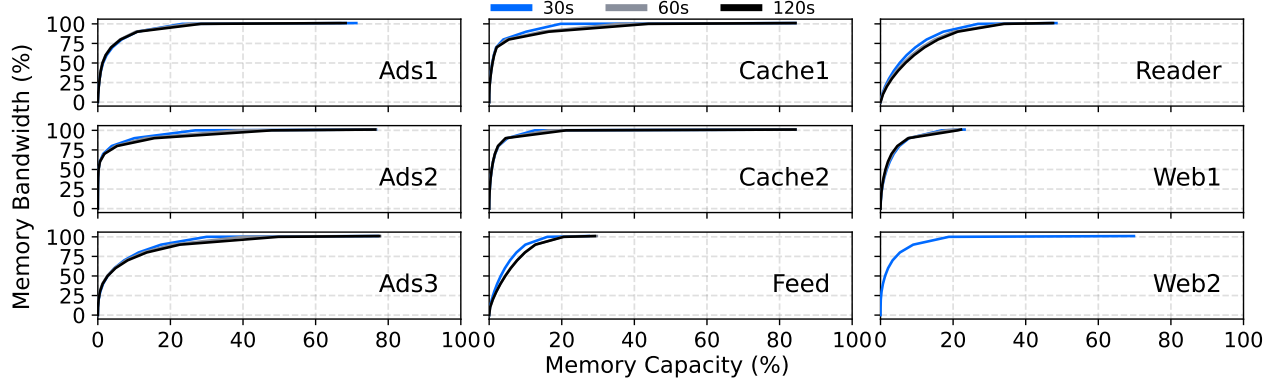


Figure 18: Memory bandwidth distribution of the workloads over three different measurement intervals.

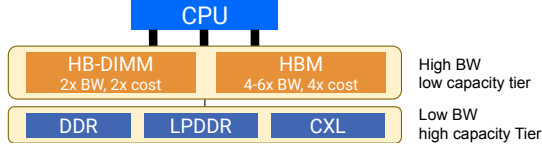


Figure 19: Mem BW tiering architectures for cloud workloads.

mainly relatively constant over time, supporting the possibility of memory bandwidth tiering.

MemProf, using its LLC demand load miss sampling, enables measuring the relative hit rate of a memory page. This is unlike current active page tracking techniques, e.g., Kernel Idle Page Tracking (IPT) [16], which only track the active pages with no visibility into how hot an active page is. Since the system does not know the “hotness” of a page, these existing techniques cannot measure the memory bandwidth distribution of a workload.

Using MemProf’s memory bandwidth distribution experiments, we make our second key observation of cloud workloads’ memory behavior:

**Key observation 2:** Only a few pages contribute to most of the memory bandwidth over varying time intervals.

Using these observations, we will study opportunities for improving system performance without adding significant cost and power overheads.

## 5.2. Memory Bandwidth Tiering

Memory bandwidth tiering enables servers with memory tiers that efficiently serve memory traffic to the high- and low-bandwidth memory pages. To explore opportunities for memory bandwidth tiering, we will look at memory technologies that support considerably higher memory bandwidth than conventional DDR-DRAM, and study their power requirements and cost overheads.

**5.2.1. Opportunities** Emerging memory technologies like High Bandwidth DIMMs (HB-DIMMs) [21] and High bandwidth memory (HBM) [28] enable memory tiers with higher than DDR bandwidth. A higher bandwidth tier in the memory hierarchy enables workloads to meet their bandwidth needs

Table 4: Capacity and theoretical peak memory bandwidth for the three memory bandwidth tiering configurations.

Config.	Near Memory	Far Memory
Baseline	100%, 100 GB/s	-
Ideal	100%, 200 GB/s (HB-DIMM like)	-
Tiered	37.5%, 200 GB/s (HB-DIMM like)	62.5%, 100 GB/s (CXL-like)

Table 5: Measured relative throughput, memory BW, and relative throughput/cost for the three configurations (Table 4).

Config	Relative Tput.	Measured BW (GiB/s)		Cost (relative)			Relative Tput./cost
		Near	Far	Near	Far	Total	
Baseline	1	67.81	-	1.0	-	1.0	1
Ideal	1.55	108.41	-	2.0	-	2.0	0.73
Tiered	1.47	84.60	19.22	0.75 (2×37.5%)	0.625 (1×62.5%)	1.375	1.13

from a small capacity memory while using DDR or CXL-based low-bandwidth, large-capacity tier to meet their memory capacity needs. HB-DIMMs provide up to 2× the bandwidth of conventional DDR5 memory but are expected to consume up to 2× the power and cost. On-package HBM [13] shows a similar trend (higher bandwidth at the expense of higher power and cost [18]).

Figure 19 shows the possible memory bandwidth tiering architecture for cloud workloads based on our observations of the nine representative workloads. While emerging memories support significantly higher memory bandwidth, this comes at increased power consumption and higher cost, making a single high bandwidth tier impractical.

**5.2.2. Evaluation** To evaluate the possibility of memory bandwidth tiering in datacenters, we will expand memory bandwidth using an HB-DIMM tier, while using a CXL-based memory tier for memory capacity (Figure 19). Please note that while we evaluate a conservative scenario with a higher memory latency far tier (CXL-based), possible memory bandwidth tiers can differ only in memory bandwidth while having similar memory latencies. For example, high-bandwidth tier using HB-DIMMs, while a low-bandwidth tier using DDR memories.

We use the three configurations listed in Table 4 for our evaluation. The baseline configuration resembles current servers

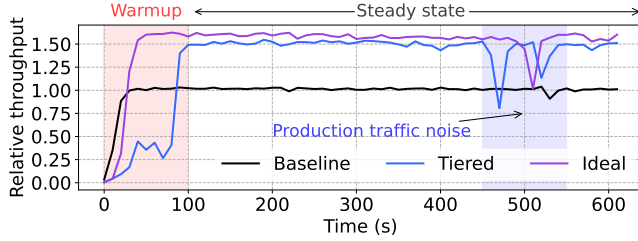


**Figure 20: Relative throughput of the Reader workload for the three memory configurations (Table 4).**

deployed in the datacenters at a hyperscaler. In contrast, the Ideal configuration shows the maximum possible performance improvement using a high-bandwidth-only tier. Finally, the Tiered configuration allocates about 1/3 of the capacity using the high-bandwidth tier that resembles HB-DIMMs, while the rest of the capacity is allocated on far memory that resembles CXL memory. The tiered configuration uses the page placement technique described by Maruf et al. [20].

We use a dual-socket server that uses DDR-5 DIMMs with configurable channel counts to allocate the memory bandwidth. Only one socket has its CPU cores enabled, with the memory connected to this socket referred to as *Near Memory*. The memory connected to the socket with all its CPU cores disabled is referred to as *Far Memory*. HB-DIMMs are expected to have DDR-5 like latencies, so we model HB-DIMMs using DDR-5 based near memory. Likewise, CXL-based memories are expected to have latency and bandwidth characteristics similar to NUMA links between the sockets [20] (Intel UPI), *Far Memory* represents a CXL-based memory tier.

**5.2.3. Results** Figure 20 shows the relative throughput of the Reader microservice serving live production traffic for the three configurations. At the steady state ( $t > 100$  s), the Tiered memory configuration achieves  $1.46\times$  better throughput than the Baseline and within 6.32% of the Ideal configuration. Out of the three configurations, the Tiered configuration takes the longest to warm up from the page migration overhead between near and far memories, which the Baseline and Ideal configurations do not have. Due to the limited and geo-restricted availability of the evaluation server machine, we only evaluate the Reader microservice, which is the most backend-bound workload out of the nine representative workloads (Figure 7).

Table 5 lists the measured memory bandwidth and relative throughput/cost for the three configurations. As HB-DIMMs are not commercially available, for our TCO analysis, we use an early assessment of HB-DIMM’s cost as  $2\times$  that of DDR-5 DIMMs. The tiered memory configuration provides a 13% improvement in performance/cost over the Baseline, and a 54.8% improvement over the Ideal configuration, making it the most cost-efficient memory hierarchy, confirming our memory bandwidth observations using MemProf.

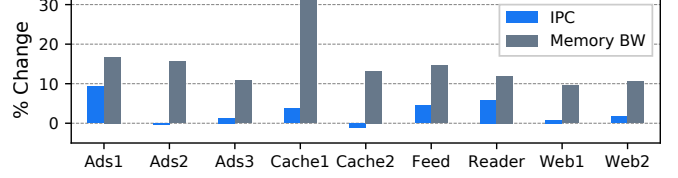


**Figure 21: IPC and mem BW change with L2 prefetchers enabled.**

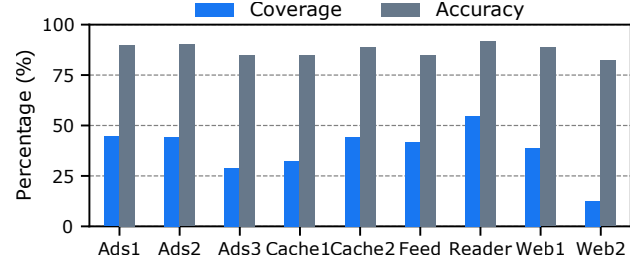


**Figure 22: L2 hardware prefetcher accuracy and coverage.**

## 6. Understanding Memory Latency

Memory latency is another significant concern for cloud workloads [2], with server processors often relying on hardware prefetchers to alleviate the performance penalty. With cloud microservices operating under strict request latency SLO constraints, workloads have to limit CPU utilization to meet the SLO guarantees, resulting in wasted resources, as discussed in Section 2.2.

A common solution to hide memory latency, the hardware prefetchers, work by prefetching soon-to-be-used cachelines, thus reducing the overall memory latency. While prefetchers hide some memory latency, they also significantly increase memory bandwidth consumption. Figure 21 shows the increase in IPC and the corresponding increase in memory bandwidth with L2 prefetchers turned on. Several workloads show a significant increase in memory bandwidth consumption (e.g., for Cache1, it increases by 31%), signalling prefetcher inefficiencies. While we present data for L2 prefetchers, from our experiments, we observe that L1 prefetchers have much higher efficiencies; thus, we omit them from our study.

Although modern hardware prefetchers monitor bandwidth utilization and throttle to reduce inefficiencies [12], we observe that workloads like Ads1 and Reader still suffer from a large memory bandwidth overhead.

Next, we will look into reasons for prefetcher inefficiencies and opportunities to mitigate them using production memory access traces.

### 6.1. Hardware Prefetcher’s Accuracy and Coverage

Figure 22 shows the accuracy and coverage of L2 hardware prefetchers for the nine workloads. Most workloads show very low coverage ( $<50\%$ ), but are relatively accurate ( $>75\%$ ). This tells us that the L2 hardware prefetcher cannot predict a large fraction of access patterns of the workloads.

Using Figure 22, we make several important observations: (a) while some workloads show negligible improvement in

	L1D Hit Ratio			R:W Ratio		
	Prod.	Trace	Error	Prod.	Trace	Error
Cache1	0.93	0.88	5.38%	1.84	1.92	-4.34%
Feed	0.95	0.93	2.11%	2.14	2.20	-2.8%
Web1	0.94	0.90	4.25%	1.72	1.67	2.3%

**Table 6: Measured (Prod.) and simulated (Trace) results.**

IPC, we keep L2 prefetchers enabled as the servers have enough memory bandwidth headroom for the listed workloads. In the past, with limited memory bandwidth, turning L2 prefetchers off has resulted in performance improvements. (b) Workloads with predictable memory access patterns (e.g., CPU-based inference) like Ads1 show a significant IPC improvement, suggesting efficient hardware prefetcher are important in improving workload performance.

While there have been proposals to improve hardware prefetchers [19, 3], research on hardware prefetchers for cloud workloads to improve their performance is limited by access to these workloads.

## 6.2. Memory Tracing for Future Architecture Research

In this section, we will look into the challenges of tracing memory accesses in a production environment; next, we will present a Pin Tool that can collect memory access traces of production workloads with low overhead. Finally, we will measure these traces’ accuracy in replicating cloud workloads’ production behavior.

## 6.3. Tracing Production Workloads

Tracing memory accesses of production workloads has several challenges that can affect the accuracy and usefulness of these traces to emulate the memory accesses offline.

*Memory tracing overhead.* Common memory tracing tools use dynamic instrumentation to trace accesses and add significant execution overhead to the application. The effect of workload slowdown is different across the different production workloads we tried to trace, with common causes being: (a) the kernel scheduler schedules some other thread on the core, (b) requests timeout, resulting in retries or failures, and (c) the load balancer reducing machine load.

*Dynamic application phases.* Tracing memory access at small granularity poses another challenge with workloads that exhibit diverse and short-lived application phases. For example, parsing a request, communicating with other microservices, or querying a database. Collecting a single small trace (millions of accesses) would not be enough to get representative behavior of the workload.

**6.3.1. Tracing Methodology** To overcome these challenges, we built a PIN Tool that can attach itself to a process, record memory access for a configurable duration (in the order of microseconds), and detaches to let the workload continue. We collect several such traces from multiple hosts and stitch them together to create a representative trace of the workload. This allows low-overhead tracing where services do not violate their request-level latency guarantees.

**6.3.2. Trace Validation** To verify the accuracy of the traces, we used a simple cache simulator with the same cache architecture as the production servers and verified the L1D hit rate. Table 6 shows the measured and simulated hit rate for the L1-D cache and the R:W ratios. All workloads show a small error, signifying that the traces are accurate for studying the memory behavior of the workloads.

## 7. Related Works

Some previous works have analyzed data center workloads code and data behavior to understand their characteristics. To the best of our knowledge, none of the prior works have looked at code sharing across threads and processes, memory bandwidth distribution of production workloads, and the impact of hardware prefetchers on memory bandwidth and performance.

Ayers et al. [2] studied the web search workload at Google and performed a detailed  $\mu$ -arch study to understand where they spent the majority of the cycles. They observe that the search workload has a large code footprint, resulting in high MPKI for the caches and propose using a large, low access-latency L4 cache. In contrast, we propose sharing L2 I-Cache and L2 I-TLB among clusters of four cores, thus increasing performance without increasing the area and power cost of the caches.

Kanev et al. [15] perform a large-scale study at Google to understand the overhead of “datacenter tax”. They make a similar observation that the I-cache is a significant bottleneck for the workloads resulting from the increasing code footprint of cloud workloads. They, however, observe that memory bandwidth consumption is fairly low across the samples because their machines have over-provisioned memory bandwidth. This is in contrast to our observations, where memory bandwidth is a growing source of concern. Despite the differences in observations, observations from MemProf are helpful in improving coverage of hardware prefetchers, resulting in possibilities for performance improvement across the board.

SoftSKU [27] characterizes cloud workloads at Meta to understand their OS and hardware behavior using “Soft SKUs”. SoftSKUs work by tuning knobs that include core/uncore frequencies, code-data prioritization for LLC, active core counts, and others. They make similar observations about the cloud workload’s IPC, cache, and TLB MPKIs. Accelerometer [26] studies the cloud workloads at Meta and observes that most cycles are spent performing tasks that are not core application logic (e.g., compression, serialization, etc).

For production traces, we ensure that they accurately represent production behavior which we validate using  $\mu$ -arch statistics. Ranganathan et al. [25] also collected traces from production. Our approach is complementary to theirs. Apart from these recent works, some earlier works [30, 5] have also looked at  $\mu$ -arch improvements for cloud workloads. A few workloads have analyzed the commercial benchmarks using similar techniques, e.g., PIN Tool [14] and top-down analy-

sis [31].

Some recent works have looked into the memory prefetcher behavior of SPEC and cloud workloads. Litz et al. [19] present critical slice prefetching (CRISP) to prefetch hard-to-predict loads using a new instruction prefix that increases the instruction's priority in the instruction scheduler. Ayers et al. [3] study SPEC and Google workloads and present an automated way of classifying memory access patterns for software-based prefetching.

We proposed a shared L2 Cache and L2 I-TLB using our observations from code sharing of production workloads. Kundu et al. [17] also studied a shared L1 cache design, but using an OLTP benchmark.

## 8. Conclusion

Memory subsystem bottlenecks are one of the primary reasons for stagnating IPC on cloud workloads. Datacenters comprise a significant part of the server processor market, but benchmarks used for CPU designs often do not represent their characteristics. In this work, we present a detailed characterization of Meta's cloud workloads using MemProf and use the findings that cores share code cachelines to propose shared L2 cache and shared L2 I-TLB caches. Next, we look into the memory bandwidth behavior of cloud workloads and evaluate memory bandwidth tiering to achieve throughput and TCO improvements. Finally, we look into ways to improve memory latency. We collect production memory traces and verify their accuracy for future memory prefetcher research.

## References

- [1] Alaa R Alameldeen and David A Wood. IPC considered harmful for multiprocessor workloads. *IEEE Micro*, 26(4):8–17, 2006.
- [2] Grant Ayers, Jung Ho Ahn, Christos Kozyrakis, and Parthasarathy Ranganathan. Memory hierarchy for web search. In *2018 IEEE International Symposium on High Performance Computer Architecture (HPCA)*, pages 643–656. IEEE, 2018.
- [3] Grant Ayers, Heiner Litz, Christos Kozyrakis, and Parthasarathy Ranganathan. Classifying memory access patterns for prefetching. In *Proceedings of the Twenty-Fifth International Conference on Architectural Support for Programming Languages and Operating Systems*, pages 513–526, 2020.
- [4] Grant Ayers, Nayana Prasad Nagendra, David I August, Hyoun Kyu Cho, Svilen Kanev, Christos Kozyrakis, Trivikram Krishnamurthy, Heiner Litz, Tipp Moseley, and Parthasarathy Ranganathan. Asmdb: understanding and mitigating front-end stalls in warehouse-scale computers. In *Proceedings of the 46th International Symposium on Computer Architecture*, pages 462–473, 2019.
- [5] Luiz André Barroso, Kourosh Gharachorloo, and Edouard Bugnion. Memory system characterization of commercial workloads. In *Proceedings. 25th Annual International Symposium on Computer Architecture (Cat. No. 98CB36235)*, pages 3–14. IEEE, 1998.
- [6] Dehao Chen, David Xinliang Li, and Tipp Moseley. Autofdo: Automatic feedback-directed optimization for warehouse-scale applications. In *Proceedings of the 2016 International Symposium on Code Generation and Optimization*, pages 12–23, 2016.
- [7] Intel Corporation. Precise events. *Intel® VTune™ Profiler User Guide*. <https://www.intel.com/content/www/us/en/develop/documentation/vtune-help/top/analyze-performance/custom-analysis/custom-analysis-options/hardware-event-list/precise-events.html>.
- [8] Intel Corporation. Code and data prioritization (CDP) technology. In *Intel 64 and IA-32 Architectures Software Developer's Manual*, volume 3B, pages 17–54 – 17–67. April 2022.
- [9] Intel Corporation. Intel® resource director technology (Intel® RDT) allocation features. In *Intel 64 and IA-32 Architectures Software Developer's Manual*, volume 3B, pages 17–50 – 17–67. April 2022.
- [10] Miyuru Dayarathna, Yonggang Wen, and Rui Fan. Data center energy consumption modeling: A survey. *IEEE Communications surveys & tutorials*, 18(1):732–794, 2015.
- [11] Jianru Ding, Ruiqi Cao, Indrajeet Saravanan, Nathaniel Morris, and Christopher Stewart. Characterizing service level objectives for cloud services: Realities and myths. In *2019 IEEE International Conference on Autonomic Computing (ICAC)*, pages 200–206. IEEE, 2019.
- [12] Wim Heirman, Kristof Du Bois, Yves Vandriessche, Stijn Eyerman, and Ibrahim Hur. Near-side prefetch throttling: Adaptive prefetching for high-performance many-core processors. In *Proceedings of the 27th International Conference on Parallel Architectures and Compilation Techniques*, pages 1–11, 2018.
- [13] Intel Corporation. Speed-up memory bandwidth bound workloads with HBM. 2022. <https://www.intel.com/content/www/us/en/high-performance-computing/hpc-high-bandwidth-memory-video.html>.
- [14] Aamer Jaleel et al. Memory characterization of workloads using instrumentation-driven simulation—a pin-based memory characterization of the spec cpu2000 and spec cpu2006 benchmark suites. *Intel Corporation*, VSSAD, 2007.
- [15] Svilen Kanev, Juan Pablo Darago, Kim Hazelwood, Parthasarathy Ranganathan, Tipp Moseley, Gu-Yeon Wei, and David Brooks. Profiling a warehouse-scale computer. In *Proceedings of the 42nd Annual International Symposium on Computer Architecture*, pages 158–169, 2015.
- [16] The Linux kernel user's and administrator's guide. Idle page tracking. [https://docs.kernel.org/admin-guide/mm/idle\\_page\\_tracking.html](https://docs.kernel.org/admin-guide/mm/idle_page_tracking.html), Feb 2015.
- [17] Partha Kundu, Murali Annavaram, Trung Diep, and John Shen. A case for shared instruction cache on chip multiprocessors running oltp. In *Proceedings of the 2003 workshop on Memory performance: Dealing with Applications, systems and architecture*, pages 11–18, 2003.
- [18] Shang Li, Dhiraj Reddy, and Bruce Jacob. A performance & power comparison of modern high-speed dram architectures. In *Proceedings of the International Symposium on Memory Systems*, pages 341–353, 2018.
- [19] Heiner Litz, Grant Ayers, and Parthasarathy Ranganathan. Crisp: critical slice prefetching. In *Proceedings of the 27th ACM International Conference on Architectural Support for Programming Languages and Operating Systems*, pages 300–313, 2022.
- [20] Hasan Al Maruf, Hao Wang, Abhishek Dhanotia, Johannes Weiner, Niket Agarwal, Pallab Bhattacharya, Chris Petersen, Mosharaf Chowdhury, Shobhit Kanaujia, and Prakash Chauhan. Tpp: Transparent page placement for cxl-enabled tiered memory. *arXiv preprint arXiv:2206.02878*, 2022.
- [21] James A McCall, Rajat Agarwal, George Vergis, and Bill Nale. High bandwidth DIMM, March 30 2021. US Patent 10,963,404.
- [22] Rick Merritt. The whales changing the industry. *EE Times*, 2019. <https://www.eetasia.com/the-whales-changing-the-industry/>.
- [23] Maksim Panchenko, Rafael Auler, Bill Nell, and Guilherme Ottoni. Bolt: a practical binary optimizer for data centers and beyond. In *2019 IEEE/ACM International Symposium on Code Generation and Optimization (CGO)*, pages 2–14. IEEE, 2019.
- [24] Milan Radulovic, Darko Zivanovic, Daniel Ruiz, Bronis R de Supinski, Sally A McKee, Petar Radojković, and Eduard Ayguadé. Another trip to the wall: How much will stacked dram benefit hpc? In *Proceedings of the 2015 International Symposium on Memory Systems*, pages 31–36, 2015.
- [25] Parthasarathy Ranganathan and Victor Lee. Advancing systems research with open-source google workload traces. <https://cloud.google.com/blog/topics/systems/workload-traces-for-google-warehouse-scale-computers>.
- [26] Akshitha Sriraman and Abhishek Dhanotia. Accelerometer: Understanding acceleration opportunities for data center overheads at hyper-scale. In *Proceedings of the Twenty-Fifth International Conference on Architectural Support for Programming Languages and Operating Systems*, pages 733–750, 2020.
- [27] Akshitha Sriraman, Abhishek Dhanotia, and Thomas F Wenisch. Softsku: Optimizing server architectures for microservice diversity@ scale. In *Proceedings of the 46th International Symposium on Computer Architecture*, pages 513–526, 2019.
- [28] JEDEC Standard. High bandwidth memory (HBM) DRAM. *Jesd235*, 16, 2013.



- [29] Manoj Sukumaran. Data center server market tracker – 2Q21 analysis. Technical report, Omdia, June 2021. <https://omdia.tech.informa.com/OM018242/Data-Center-Server-Market-Tracker--2Q21-Analysis>.
- [30] Pedro Trancoso, J-L Larriba-Pey, Zheng Zhang, and Josep Torrellas. The memory performance of dss commercial workloads in shared-memory multiprocessors. In *Proceedings Third International Symposium on High-Performance Computer Architecture*, pages 250–260. IEEE, 1997.
- [31] Ahmad Yasin. A top-down method for performance analysis and counters architecture. In *2014 IEEE International Symposium on Performance Analysis of Systems and Software (ISPASS)*, pages 35–44. IEEE, 2014.